



**Silesian University of Technology**  
**Faculty of Chemistry**  
**Department of Physical Chemistry and**  
**Technology of Polymers**



Welisson de Pontes Silva

**DOCTORAL DISSERTATION**

*Design, Synthesis, and Investigation of the Photophysical and  
Electrochemical Properties of Selected Conjugated Molecules Belonging  
to Various Classes of Compounds*

Promoter: Prof. Dr hab. inż. Mieczysław Łapkowski

Assistant Promoter: Dr inż. Radosław Motyka

Gliwice 2023

## Extended Abstract

### Introduction

The society is largely dependent on artificial light. It shows the importance of searching for more technologies related to eco-friendly sources to increase life quality and reduce energy consumption in our society. Recently, research in the field of optoelectronics has focused on organic light-emitting diodes (OLEDs) and organic photovoltaic (OPV) solar cells, which appear as an alternative strategy to achieve efficient light emitters and energy generation.<sup>1</sup> The future of the lighting market is searching for more efficient devices that can operate at lower voltages and have a wide range of accessible colors.  $\pi$ -Conjugated organic materials have been used in electronic devices and presented excellent results concerning typical inorganic semiconductors, which generally contain expensive and rare heavy metals. The flexibility and processability that organic materials can offer to electronic devices minimize the costs and increase the possibilities of applications in the electronics industry due to the versatility of functionalization that can be made in conjugated organic molecules. Organic materials can already be encountered in commercial OLED, OPVs, and organic field effect transistors (OFET). The versatility of  $\pi$ -conjugated organic materials consists in the possibility of using them as active organic layers simultaneously in diodes, transistors, solar cells, and others.<sup>2,3</sup> In this context, searching for new materials that can attend to the parameters necessary to be applied in such devices with high efficiency, color purity, and stability is still challenging. Also, other applications such as OPVs and OFETs had the necessity of designing and synthesizing more and more materials to understand the mechanisms involved and improve the efficiency. In this way, the design and synthesis of new conjugated organic compounds is the future of this field. In this way, this thesis focuses on the design and synthesis of new ambipolar compounds as candidates to be applied as organic electronic materials, especially to OLED devices. In addition, the photophysical and electrochemical characterizations performed will give an understanding of the mechanisms involved in light generation.

### Background theory

Research in the mechanisms of light emission by organic compounds is fundamental to the rational design for optoelectronic applications. The light emission in response to the absorption of energy is called luminescence. This process can occur when a molecule absorbs a necessary quantity of energy to promote electronic transitions from the ground state to the excited state. In sequence, when the excited molecule relaxes to the fundamental state by radiative decay, it could happen with light emission. The excitation of the molecule can occur in different ways, such as chemical reactions (chemiluminescence), electric excitation (electroluminescence), and absorption of light (photoluminescence).<sup>4</sup> An OLED is a light-emitting diode (LED) that incorporates organic compounds as an emitter layer within its structure, enabling light emission through excitation by an electric current.<sup>5</sup> OLED device structures have presented numerous modifications since the initial reports. Typically, the

construction involves a thin organic emitting layer that is sandwiched between two electrodes, with one of them being transparent.

Three generations of OLEDs have been developed in parallel, aiming to construct efficient and low-cost devices (**Figure 1**). The first and second generations of OLED devices had limitations. The first was related to efficiency because all the light came from singlet excitons, which is theoretically limited to 25%, which can achieve EQEs up to 5% in the device. The emission layer in this kind of device presented a  $\pi$ -conjugated molecular design with a rigid chemical structure and good thermal stability. The challenges are related to the aggregation causes quenching in the solid state, which may result in weakly emissive systems due to effective molecular  $\pi$ -stacking and attractive dipole-dipole interactions.<sup>5</sup> The second-generation (phosphorescent OLEDs) was based on the remaining 75% of triplet excitons. These devices are typically based on phosphorescent heavy metal complexes. Heavy metal atoms, such as Iridium or platinum, can enhance the spin-orbit coupling (SOC) and facilitate the process of Intersystem Crossing (ISC). If the ISC is very effective, the singlet excitons can be used to achieve 100% IQE. However, the challenge with phosphorescent OLEDs is the necessity to use expensive and scarce metals to obtain them.<sup>6,7</sup> The third generation of OLEDs is based on a delayed fluorescence process. The strategy to increase the device's efficiency is to use mechanisms to harvest triplets to singlet states to achieve 100% IQE. For that, the reverse intersystem crossing (RISC) from triplet ( $T_1$ ) to singlet ( $S_1$ ) states need to be effective to have an efficient delayed fluorescence process.<sup>8</sup> The mechanism to harvest triplets to singlets states is possible by Thermally Activated Delayed Fluorescence (TADF). This mechanism can be achieved with the use of purely organic emitters. Because of that, various research groups focus on the design and synthesis of TADF emitters to be applied in organic light emitting devices.<sup>9</sup>

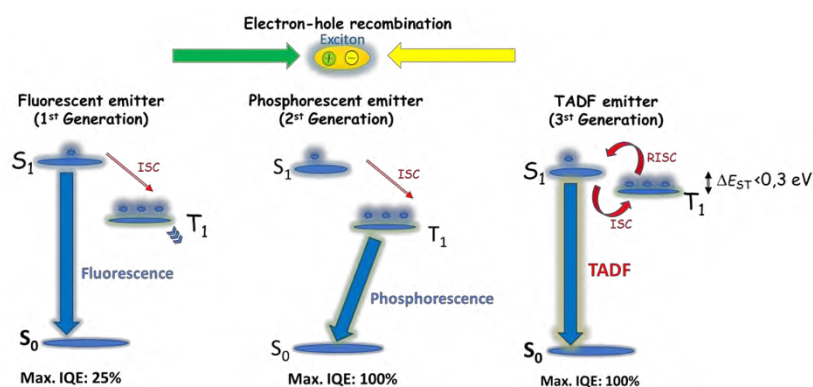


**Figure 1.** Generations of OLEDs devices. Adapted from literature.<sup>5</sup>

The delayed fluorescence (DF) process can occur by two mechanisms (**Figure 1** **Error! Reference source not found.**). The first E-type delayed fluorescence (or Thermally Activated Delayed Fluorescence – TADF) is associated with the energy between the singlets and triplets states. This energy gap needs to be very small ( $\Delta E_{ST} < 0.3$  eV). In these conditions, the excited molecules in triplets states can move to singlets states by reverse intersystem crossing (RISC). The RISC process is thermally

supported by the proper energy from the molecule by an intense charge transfer process. The maximum efficiency of this mechanism can achieve 100%. The second P-type delayed fluorescence (Triplet-Triplet Annihilation -TTA) is associated with two molecules in the excited triplet state that can annihilate to yield one molecule in the ground state ( $S_0$ ) and one in the excited singlet state ( $S_1$ ) (triplet fusion), that can relax to the ground state by emission of photons in the delayed fluorescence mechanism. The main problem with this process is related to the low (less than 50%) efficiency.<sup>5,7</sup>

Designing new TADF compounds is a challenging task involving several essential conditions simultaneously.<sup>10</sup> These conditions include:

a) the minimization of the energy gap ( $\Delta E_{ST}$ ) between the singlet and triplet excited states; b) Minimizing non-radiative decay pathways to ensure that the triplet excited state persists for an extended lifetime, improving the probability of efficient triplet harvesting through the thermally activated reverse intersystem crossing (RISC) mechanism; c) Maximizing the photoluminescence quantum yield (PLQY).

The reduction of  $\Delta E_{ST}$  is fundamental in maximizing the rate constant RISC ( $k_{RISC}$ ), as indicated by the equation in dependence of temperature:  $k_{RISC} \propto e^{\frac{-\Delta E_{ST}}{k_B T}}$ , where  $k_B$  is Boltzmann constant and T is the temperature. From this equation, we can observe that for higher  $\Delta E_{ST}$ , we will have the lower value of  $k_{RISC}$ , and vice versa.<sup>11</sup> Therefore, the molecular design to obtain molecules with TADF properties is based on the balance of control of the bandgap values, such as HOMO-LUMO and singlet-triplet energy that are related to the light emission wavelength, the PLQY, and the efficiency of RISC process.<sup>8,12</sup>

The development of new organic materials based on TADF properties is based on the synthesis of ambipolar compounds, but not only in specific standard D-A arrangements. The ambipolar compounds can present different arrangements such as Donor-Acceptor (D-A), Donor-Acceptor-Donor (D-A-D), Donor- $\pi$ -spacer-Acceptor- $\pi$ -spacer-Donor (D- $\pi$ -A- $\pi$ -D), D<sub>3</sub>-A, D<sub>3</sub>- $\pi$ -A, D<sub>4</sub>-A and others arrangements that can present intense intermolecular charge transfer (ICT) process, mediating the  $\Delta E_{ST}$  to achieve thermally activated RISC process.<sup>13,14</sup>

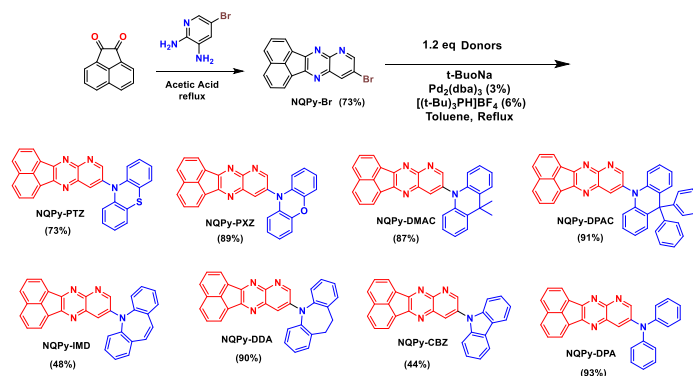
Further investigations become necessary to find structures with balanced, efficient RISC and PLQY values. These parameters can be obtained in systems with strong acceptors and several weaker donors, for example, in D-A-D, and D<sub>3</sub>A configurations, to increase the donor character in the structures. Recently, the control of  $\Delta E_{ST}$  was also performed in systems with a multi-resonance effect.<sup>15</sup> Additionally, the extension of the  $\pi$ -conjugation degree and the redox potentials are also crucial in the design of efficient TADF compounds. Which can help to cover the emission wavelength in the visible region from blue to red with stability and color purity.<sup>16</sup>

***D-A compounds derived from Pyridoquinoxalines: Synthesis and investigation of Photophysical and electrochemical properties***

Materials based on quinoxaline core have been largely investigated for application in optoelectronic devices due to the high level of charge transport carriers and intrinsic high photoluminescence quantum yields (PLQY).<sup>17,18</sup> Pyridoquinoxalines presented a higher acceptor character in relation to quinoxalines due to the addition of one more nitrogen atom in the system that increases the electronegativity in the core. Ambipolar compounds based on quinoxalines as acceptor and common donor units were used to obtain efficient TADF materials.<sup>19–21</sup> The synthetic versatility of the pyridoquinoxalines family are very attractive due to the easy synthetic approach by a condensation reaction of 2,3-diaminopyridines and dicarbonyl derivatives, being simple and low cost. Various substituents can be used in the diaminopyridines and in the dicarbonyl part in order to functionalize the core. Different D-A molecules based on this system were investigated to obtain multifunctional materials.<sup>22,23</sup> Although, the dicarbonyl based on acenaphto-1,2-dione were not much investigated so far,<sup>24</sup> the naphthalene endow them with rigid planar structure, with abundant delocalization of the  $\pi$  electrons. In this way the condensation with acenaphto-1,2-dione can be an excellent strategy to obtain a new core aiming multifunctional properties.

In this way, this chapter is based on the design, synthesis, and investigation of the photophysics and electrochemistry properties of one new series of compounds based on acenaphtopyridoquinoxaline as acceptor core and donor units such as carbazole, diphenylamine, phenothiazine, phenoxazine, acridine derivatives and azepine derivatives in order to define the relation between molecular structure and photophysical properties to be applied in OLEDs devices with high range of accessible colors.

The designed compounds were synthesized in two steps according to **Scheme 1**. The structures of all compounds were confirmed by nuclear magnetic resonance (NMR) spectroscopy and High-Resolution Mass Spectrometry (HRMS).



**Scheme 1.** Synthetic routes to obtain NQPy-Donors. Donors: PTZ, PXZ, DMAC, DPAC, IMD, DDA, CBZ and DPA.

The electrochemical properties of the **NQPy-Donors** were investigated by cyclic voltammetry (CV) to estimate the HOMO and LUMO energy levels. The estimated ionization potential (IP) and electron affinity (EA) (from onset oxidation ( $E_{ox}$ ) and reduction ( $E_{red}$ ) potentials), are correlated with the HOMO ( $E_{HOMO}$ ) and LUMO ( $E_{LUMO}$ ) energy levels, respectively, using the following equations:  $E_{HOMO} = -(E_{ox} + 5.1)$ ;  $E_{LUMO} = -(E_{red} + 5.1)$ .<sup>25</sup> The results are summarized in **Table 1**.

**Table 1.** Electrochemical parameters obtained by CV measurements and DFT calculations.

Compound	Cyclic Voltammetry <sup>a</sup>			Theory <sup>b</sup>		
	HOMO (eV)	LUMO (eV)	$E_g$ (eV)	HOMO (eV)	LUMO (eV)	$E_g$ (eV)
NQPy-PTZ	-5.49	-3.45	2.04	-5.79	-3.68	2.11
NQPy-PXZ	-5.56	-3.56	2.00	-5.79	-3.68	2.11
NQPy-DMAC	-5.68	-3.44	2.24	-5.95	-3.62	2.33
NQPy-DPAC	-5.77	-3.44	2.33	-6.00	-3.64	2.36
NQPy-DDA	-5.90	-3.19	2.69	-6.04	-3.56	2.48
NQPy-IMD	-5.87	-3.18	2.71	-6.13	-3.53	2.60
NQPy-CBZ	-6.01	-3.49	2.52	-6.27	-3.60	2.77
NQPy-DPA	-5.85	-3.41	2.44	-6.08	-3.40	2.68

<sup>a</sup> Measurements were performed for 1 mM solutions of investigated compounds in the presence of 100 mM tetrabutylammonium tetrafluoroborate and calibrated using ferrocene/ferrocenium redox couple. <sup>b</sup> Results obtained at the B3LYP/6-31G\*\* level of theory.

All materials showed good stability and reversibility in the applied voltage range specially in the reduction process concerned in the acenaphthopyridoquinoxaline unit. The LUMO levels of the investigated compounds did not present many differences in the values. But appears to be affected by a partial conjugation with the donor and hence it varies according to its type. The first oxidation process was more clear reversible for **NQPy-PTZ** and **NQPy-PXZ**. While it was more irreversible for the other compounds. The donor character of the materials can be evaluated considering the HOMO levels energy varying with **NQPy-CBZ** < **NQPy-DDA** < **NQPy-IMD**, **NQPy-DPA** < **NQPy-DPAC** < **NQPy-DMAC** < **NQPy-PXZ** < **NQPy-PTZ**. The electrochemical band ( $E_g$ ) gap follows the small values for D-A combinations with the acceptor and strong donors, while for the compounds with less strength electron donation the  $E_g$  increases. The results obtained by DFT calculations show a good correlation with the experimental electrochemical data as we can observe in the **Table 1**.

The results of photoluminescence in solution are summarized in **Table 2** **Error! Reference source not found.**. Analyzing the PL spectra we can observe emission for all compounds, except for **NQPy-PXZ** in DCM. Which can be attributed to the polarity of the DCM that could stabilize the <sup>1</sup>CT excited state leading to a quench of the emission.<sup>26,27</sup> All the compounds showed CT (with gaussian profile) or CT+LE (with vibronic profile) emission in solution.

**Table 2.** Summary of photophysical characteristics of the studied D-A luminophores.

Compounds	$\lambda_{abs}/nm$ [ $\epsilon/10^3 M^{-1} cm^{-1}$ ] <sup>a</sup>	$\lambda_{em}$ [nm]	$\lambda_{em}$ [nm]	PLQY [%] DCM/TOL
		DCM	Toluene	
NQPy-PTZ	322 [30.1], 418 [8.4], 485sh [2.6]	518	476, 656	<1/<1
NQPy-PXZ	322 [63.9], 472 [2.3], 566sh [0.8]	-	638	-/1.7
NQPy-DMAC	322 [80.4], 447 [3.9]	657	580	<1/19.1
NQPy-DPAC	322[14.2], 440 [1.3]	627	557	3.8/26.5
NQPy-DDA	307 [25.1], 348 [16.2], 426 [12.5]	500, 624	473, 545	10.3/31.2
NQPy-IMD	304 [31.2], 345 [21.2], 417 [14.8]	495	472	2.9/11.8
NQPy-CBZ	292[10.4], 317 [19.0], 419 [4.76]	537	485	81.9/43.8
NQPy-DPA	312 [69.7], 351 [24.6], 444 [26.3]	581	529	77.5/99.6

<sup>a</sup> Absorption spectra recorded in DCM solutions  $1 \times 10^{-5}$  M.

The compounds **NQPy-PTZ**, **NQPy-PXZ**, **NQPy-DMAC** and **NQPy-DPAC** presented an increment in emission intensity in degassed measurements indicating that the molecules can present mechanisms involving the triplet states which are consistent with TADF properties. The compounds **NQPy-DMAC** and **NQPy-DPAC** showed the high values in the emission increment, 1.8x and 2.5x, respectively, which can be associated with more efficient RISC process for these compounds.

To better understand the optical properties of the **NQPy-donors** compounds in the aggregate state, we investigate the photoluminescent behavior in THF/water mixtures with different water fractions ( $f_w$ ) at 100  $\mu$ M concentration. The experimental results and photographs (**Figure 2**) show that the emission spectra of the compounds shows different behavior in THF/water mixtures. **NQPy-PTZ** and **NQPy-PXZ** display low emission in THF solutions, while the emission is increased upon addition of water ( $f_w = 80-90\%$ ) indicating evident aggregation induced emission enhancement (AIEE) behavior. Additionally, we have observed that **NQPy-PXZ** has a very low PLQY in toluene, around 2%, and an even lower photoluminescence yield in DCM or THF. However, we noticed that the PL intensity of **NQPy-PXZ** increases up to 50 to 100-fold upon precipitation. This indicates that **NQPy-PXZ** exhibits AIE behavior rather than AIEE.<sup>28</sup> We can observe that **NQPy-DMAC**, **NQPy-DPAC**, and **NQPy-DPA** show an interesting behavior, where an initially relatively strongly luminescent THF solution displays significantly lower PL intensity, near complete quenching, upon initial addition of water. This behavior can be interpreted as CT PL quenching due to increases of solvent polarity caused by addition of highly polar water. Addition of further amounts of water induces a relative increase in PL intensity by ~100-900 fold, which is commonly interpreted as AIE.<sup>28</sup> **NQPy-DDA**, **NQPy-IMD**, and **NQPy-CBZ**, showed a similar behavior to **NQPy-DMAC**, **NQPy-DPAC**, and **NQPy-DPA**, however the overall increase in PL intensity upon aggregation ( $f_w > 60\%$ ) is lower. Importantly, for **NQPy-CBZ** we observe PL intensity at high water content to be significantly lower than in dry THF, an effect in line with aggregation caused quenching (ACQ). For the compounds **NQPy-DMAC** and **NQPy-DPAC** we observe a blue shift in the luminescence at high  $f_w = 80-90\%$  related to THF solution. This behavior can be interpreted as an effect of molecular interactions between fluorophores being less strong than with the solvent when completely dispersed in a solution. In addition, aggregate environment is much more rigid than solution, what can also contribute to the PL blue shift.<sup>29-31</sup>

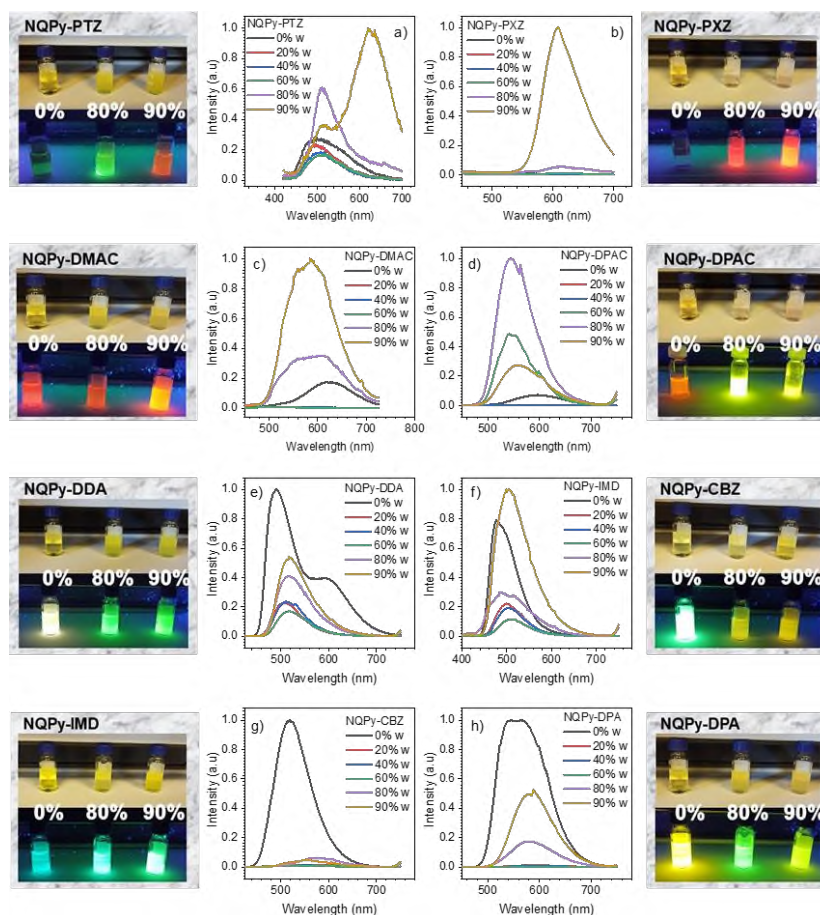


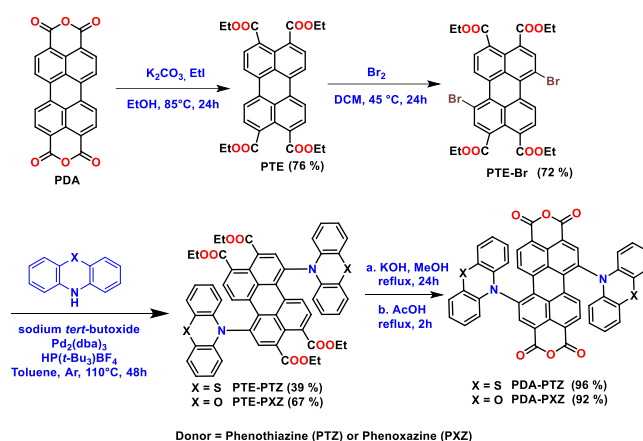
**Figure 2.** a-g) Emission spectra recorded in THF/water mixtures for water fractions  $fw = 0$ -90%. On the sides photographs of solutions and dispersions of the NQPy-Donors compounds in THF ( $fw = 0\%$ ) and THF/water mixtures,  $fw = 80$ -90 %. Top images show photographs under ambient light, while the bottom was recorded with UV light illumination.

### New D-A-D compounds derived from Perylene: design, synthesis and characterization

Perylenes are important class of compounds that present a high level of  $\pi$ -conjugation. Materials containing derivatives of perylene have been largely applied in strategies to obtain organic photovoltaic cells (OPVs),<sup>32</sup> liquid crystals (LC),<sup>33</sup> photo-emissive materials,<sup>34</sup> sensors,<sup>35</sup> and others.<sup>35-37</sup> Devices based on OLEDs, OPVs, and organic field effect transistors (OFETs) are very important in nowadays and researches focusing on the use of perylene core can be an excellent strategy to get smart materials with multifunctional properties due the tuning of photophysical and electrochemical parameters.<sup>38</sup> The investigations in perylenes derivatives for TADF systems were not so explored in the literature yet, which open new challenges to investigations using this acceptor core combined with different donor moieties. Perylene dianhydride (PDA) cores are very attractive due to their versatility to perform functionalization by different types of organic reactions and the usability of the photophysical properties in optoelectronic applications, due to its exceptional photochemical stability, strong and broad absorption in the visible region.<sup>39</sup>

The structures were thought to present the perylene core with donor units attached in order to favor CT process by spatial separation of HOMO-LUMO. Also, the donors attached can help in the increment of solubility in the standard PDA system, due to the twisted conformation presented for the materials. The phenothiazine and phenoxazine donors were chosen due to the higher electron donation ability in order to equilibrate the higher electron deficiency from PTE and PDA systems.

The synthesis of the new materials derived from perylene follows **Scheme 2**. The first step of reaction was the esterification of **PDA** to obtain the compound **PTE**. The bromination of **PTE** provides the mix of isomers (mono and dibrominated compounds) that were isolated by column chromatography to give the compound **PTE-Br**. With **PTE-Br** was possible to realize the N-C coupling. The reactions were performed using the respective donor unit (PTZ or PXZ) to obtain the compounds **PTE-Donors** in moderate yields (40%) after purification by column chromatography. The last step was performed the hydrolysis reaction of **PTE-Donors** to obtain the compounds **PDA-Donors** in quantitative yields.



**Scheme 2.** Synthetic route to obtain the compounds **PDA-PTZ** and **PDA-PXZ**.

The electrochemical properties of the **PTE-Donors** and **PDA-Donors** were investigated by cyclic voltammetry (CV) to estimate the HOMO and LUMO energy levels (Table 3 Table 3. Electrochemical parameters obtained by CV measurements and DFT calculations.).

**Table 3.** Electrochemical parameters obtained by CV measurements and DFT calculations.

Compounds	Cyclic Voltammetry <sup>a</sup>			Theoretical calculations <sup>b</sup>		
	HOMO (eV)	LUMO (eV)	E <sub>g</sub> (eV)	HOMO (eV)	LUMO (eV)	E <sub>g</sub> (eV)
<b>PTE-PTZ</b>	-5.42	-3.75	1.67	-5.88	-3.95	1.93
<b>PTE-PXZ</b>	-5.51	-3.81	1.70	-5.83	-4.01	1.82
<b>PDA-PTZ</b>	-5.55	-4.50	1.05	-6.32	-4.89	1.43
<b>PDA-PXZ</b>	-5.69	-4.53	1.16	-6.18	-4.94	1.24

<sup>a</sup> Measurements were performed for 1 mM solutions of investigated compounds in the presence of 100 mM tetrabutylammonium tetrafluoroborate and calibrated using ferrocene/ferrocenium redox couple. <sup>b</sup> theoretical calculations obtained at B3LYP/6-31G\*\* level of theory.

The investigated compounds showed very good stability and reversible electrochemical response in the applied voltage range. All molecules were characterized by a one-step, reversible

oxidation process involving phenoxazine (PXZ) or phenothiazine (PTZ) donor unit and a stable, reversible two-step reduction process which is typical for the 1,7 disubstituted PTE and PDA derivatives.<sup>40</sup> The HOMO energy values did not show many differences, presenting slightly higher values for PDA derivatives. On the other hand, the LUMO energy was greatly influenced by the interconversion reaction of **PTE-PTZ** and **PTE-PXZ** (-3.75 eV and -3.81 eV, respectively) to **PDA-PTZ** and **PDA-PXZ** (-4.50 eV and -4.53 eV, respectively), showing higher values for PDA-Donors which indicates the easy reduction for these compounds. This behavior leads to lower HOMO-LUMO gaps ( $E_g$ ) for **PDA-donors** around 1 eV (1.05 eV for **PDA-PTZ** and 1.16 eV for **PDA-PXZ**) in comparison to **PTE-donors** (1.67 for **PDA-PTZ** and 1.70 for **PDA-PXZ**). Other behavior related to donor strength was observed, where the PTZ derivatives showed lower  $E_g$  in relation to PXZ derivatives.

***Asymmetric D-A-D compounds derived from naphthalene benzimidazole: design, synthesis, photophysical and electrochemical properties***

The naphthalene benzimidazole is a very interesting N-rich acceptor due to the increase of electronegativity by addition of carbonyl group conjugated with the imidazole system.<sup>32</sup> The naphthalene part is responsible for increment in the  $\pi$ -conjugation degree which contributes to minimization of the HOMO-LUMO gap.<sup>41</sup> The asymmetric core with the bromines in 4,7-positions of the benzimidazole part is a very interesting synthetic strategy allowing for functionalization by addition of different donor moieties. These bromines can be subjected to different types of reactions with emphasis on N-C coupling and C-C coupling.

Therefore, in this part of the work, the design, synthesis, and study of the photophysical and electrochemical behavior of a new series of compounds based on the asymmetric naphthalene benzimidazole as an acceptor core and phenothiazine, phenoxazine, and diphenylamine as donor units are described. Additionally, a phenyl  $\pi$ -spacer group was introduced between the donor and acceptor units to study the relationship between the molecular structure and photophysical and electrochemical properties.

The synthetic routes used to obtain the final molecules are shown in **Scheme 3****Error! Reference source not found.** First, **BTZ** core was opened by a reduction reaction to obtain the compound **BTZ-NH<sub>2</sub>** in good yields. The diamino compound was used in the next step in the condensation reaction with 1,8-naphthaleneanhydride to obtain the compound **BTNA-Br<sub>2</sub>**. The N-C coupling was performed using two equivalents of phenothiazine as a donor to obtain the compound **BTNA-PTZ** in moderate yields. To perform the Stille C-C coupling reactions it was necessary to prepare the Stille reagent in advance. The Stille derivatives obtained reacted with the **BTNA-Br<sub>2</sub>** core in the presence of the Palladium-tetrakis(triphenylphosphine) as a catalyst giving the compounds **BTNA-*p*-PTZ**, **BTNA-*m*-PTZ**, **BTNA-*p*-PXZ** and **BTNA-*p*-DPA**. All newly synthesized compounds were fully characterized by <sup>1</sup>H and <sup>13</sup>C Nuclear Magnetic Resonance (NMR) and by High-Resolution Mass Spectrometry (HRMS) for the final molecules.



occurring on the donor units. The LUMO levels of the investigated compounds presented notable differences in the values, varying from -3.25 eV to -3.75 eV, depending on the donor coupled and by insertion of the phenyl spacer between naphthalene benzimidazole core and donor. The reversibility in the reduction process is notable for all compounds suggesting the electrochemical stability of the **BTNA** core. The oxidation process also showed reversibility, and appeared at least as two steps oxidation process, which can be related to the presence of two donor moieties. The first oxidation process was notably reversible for all compounds. The compounds also showed second step oxidation with reversibility for **BTNA-p-PTZ**, **BTNA-PTZ** and **BTNA-p-DPA**. On the other hand, it was not reversible for **BTNA-m-PTZ** and **BTNA-p-PXZ**. **BTNA-p-DPA** and **BTNA-PTZ** showed the two oxidation steps very close, being merged. The electrochemical band gap ( $E_g$ ) showed the lowest value for the compound without the phenyl spacer group (**BTNA-PTZ**, 1.76 eV), indicating the lower  $\pi$ -conjugation degree for this compound.

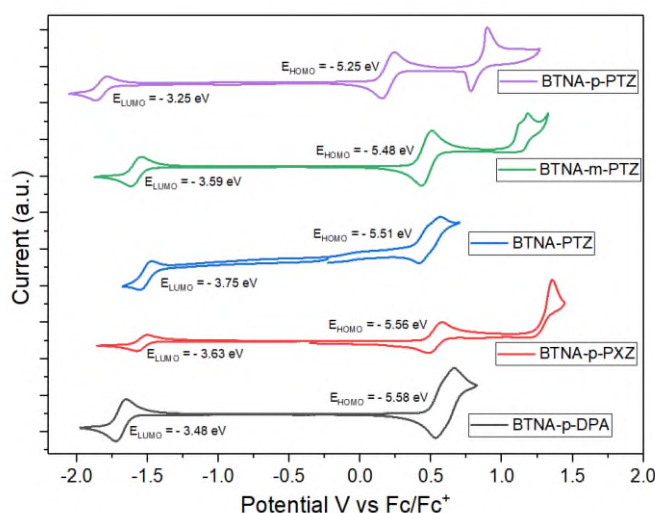


**Figure 3.** Voltammograms of the 1mM solutions of compounds **BTNA-Donors** in 100mM tetrabutylammonium tetrafluoroborate in DCM.

**Table 5** summarizes the photophysical properties of the **BTNA-donors**. The PL spectra of **BTNA-PTZ** showed two emission bands centered at  $\lambda_{\text{PL}} = 479$  (more intense) and  $\lambda_{\text{PL}} = 610$  nm (less intense). This behavior can be attributed to the possibility of two  $^1\text{CT}$  states by the asymmetry of the naphthalene benzimidazole core, with two units of phenothiazine given different CT states.<sup>42</sup> Additionally, due to possibility of two  $^1\text{CT}$  states by phenothiazine donor assuming two stable conformations, such as *quasi*-axial and *quasi*-equatorial, which also results in two distinct CT energies.<sup>43</sup> The compound **BTNA-p-PTZ** (with phenyl  $\pi$ -spacer group) also showed two emission peaks centered at  $\lambda_{\text{PL}} = 542$  and  $\lambda_{\text{PL}} = 577$  nm attributed to the previous explanation. The red shift in the first peak (compared to **BTNA-PTZ**) is related to the increase of the  $\pi$ -conjugation degree by the addition of phenyl spacer group. Comparing the *para* and *meta* positions (**BTNA-m-PTZ**) we observe a red shift in the emission due to the character of electron-donation from phenothiazine in meta position be

decreased. The compounds **BTNA-*p*-PXZ** showed vibronic emission with maximum emission wavelength  $\lambda_{PL}$  = 583 nm. On the other hand, **BTNA-*p*-DPA** clearly showed CT character due the gaussian profile of emission with maximum  $\lambda_{PL}$  = 594 nm.

**Table 5.** Photophysics properties of the compounds **BTNA-donors** in solution and in zeonex matrix.

Compounds	$\lambda_{abs}/nm$ [ $\epsilon/10^3M^{-1}cm^{-1}$ ] <sup>a</sup>	$\lambda_{em}/nm$ <sup>b</sup>	PLQY <sup>c</sup> (%)	Increase	PLQY x Increase (%)
<b>BTNA-<i>p</i>-PTZ</b>	258 [33.6], 314 [11.4], 398 [4.5]	542, 577	13.7	1.12	15.3
<b>BTNA-<i>m</i>-PTZ</b>	258 [34.7], 294 [11.5], 310 [11.6], 395 [4.8]	578, 595	15.3	1.66	26.0
<b>BTNA-<i>p</i>-PXZ</b>	240 [44.7], 270 [10.1], 315 [13.7], 394 [5.5]	553, 583	16.4	1.15	18.9
<b>BTNA-<i>p</i>-DPA</b>	232 [24.4], 303 [20.0], 363 [20.4], 465 [2.8]	594	8.3	1.09	9.1
<b>BTNA-PTZ</b>	257 [30.2], 289 [6.6], 301 [7.6], 381 [5.6]	479, 610	<1	1.26	1.1

<sup>a</sup> Absorption measured in DCM 0.01 mM. <sup>b</sup> Obtained from zeonex matrix. <sup>c</sup> obtained in zeonex matrix.

The materials showed moderate PLQYs, where **BTNA-*p*-PXZ** presents the highest value (16.4%). All the compounds showed an increase in the emission intensity under vacuum conditions, which indicates that triplet states are involved in the emission mechanism, which is characteristic of TADF behavior.

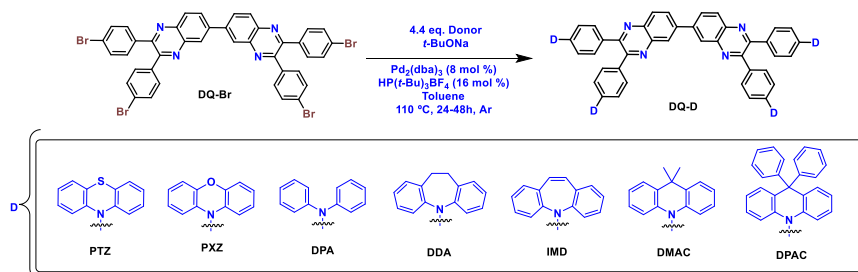
#### ***New D-A-A-D compounds derived from flexible/rigid diquinoxalines/phenazines: design, synthesis, photophysical and electrochemical properties***

Quinoxalines are important materials that present a high conjugation degree, good charge carriers transport and high electron-acceptor character.<sup>44</sup> The presence of the nitrogen atoms in the aromatic system increases the electron-acceptor properties, additionally they can be modulated by the number of quinoxaline rings in the molecular structure. Quinoxalines can be obtained in very good yields by dehydration reactions between *ortho*-diamino compounds and aromatic dicarbonyl compounds.<sup>23</sup> Therewith the design of TADF based materials can be made using different quinoxalines. The non-planarity in the diquinoxaline core induces different behavior in photophysical properties considering the possible conformations in these systems.

Herein, we designed and synthesized a new series of compounds based on flexible diquinoxaline (**DQ** core) or rigid bidibenzo[*a,c*]phenazine (**NQ** core) as acceptors and different donor moieties. The flexible diquinoxaline (DQ) allows the free rotation of the phenyl spacer between the acceptor and the four donor moieties. On the other hand, the NQ core, did not present a phenyl spacer between the donor

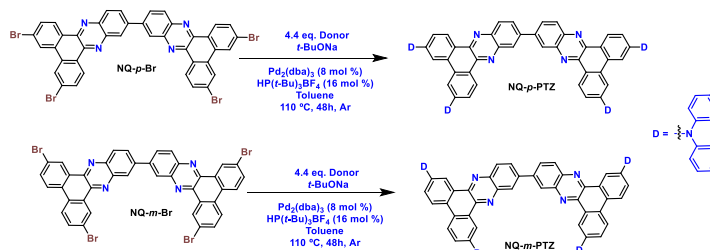
and acceptor system. These characteristics make it possible to obtain different photophysical behavior by the control of arrangement in the molecular structures.

**DQ-Br** was synthesized by condensation reaction of 4,4'-dibromobenzil and 3,3'-diaminobenzidine. The rigid bisphenazines with bromine in *para* (**NQ-*p*-Br**) and *meta* (**NQ-*m*-Br**) positions were synthesized in a similar way, using the dicarbonyl compounds 3,6-dibromophenanthrene-9,10-dione<sup>45</sup> and 2,7-dibromophenanthrene-9,10-dione,<sup>46</sup> respectively. The next step was based on a nitrogen-carbon coupling reaction catalyzed by palladium as shown in **Scheme 4**. The reactions were performed with degassed toluene as a solvent using different donor units (phenothiazine, phenoxazine, diphenylamine, azepine and acridine derivatives) to obtain the final compounds **DQ-PTZ**, **DQ-PXZ**, **DQ-DPA**, **DQ-DDA**, **DQ-IMD**, **DQ-DMAC** and **DQ-DPAC** in moderate to good yields after purification by chromatography column and precipitation in methanol.



**Scheme 4.** Synthetic route to obtain the **DQ-Donors**.

For the bisphenazine acceptors **NQ-*p*-Br** and **NQ-*m*-Br**, phenothiazine was used as donor units with similar procedures to **DQ-Donors** of the N-C coupling reaction obtaining the final **NQ-*p*-PTZ** and **NQ-*m*-PTZ** in moderate yields after purification by chromatography column (**Scheme 5**).



**Scheme 5.** Synthetic route to obtain the **NQ-*p*-PTZ** and **NQ-*m*-PTZ**.

The electrochemical properties of the compounds were investigated by cyclic voltammetry (CV) to estimate the HOMO and LUMO energy levels. The results are summarized in **Table 6** and the voltammograms in **Figure 4** and **Figure 5**.

**Table 6.** HOMO and LUMO energy levels estimated from CV measurements of **DQ-Donors** and **NQ-Donors**.

Compound	Cyclic Voltammetry <sup>a</sup>		
	HOMO (eV)	LUMO (eV)	$E_g$ (eV)
<b>DQ-PXZ</b>	-5.39	-3.32	2.07
<b>DQ-DPA</b>	-5.40	-3.15	2.25

<b>DQ-IMD</b>	-5.82	-3.34	2.48
<b>DQ-DDA</b>	-5.65	-3.32	2.33
<b>DQ-DMAC</b>	-5.68	-3.54	2.14
<b>DQ-DPAC</b>	-5.91	-3.65	2.26
<b>DQ-PTZ</b>	-5.35	-3.32	2.03
<b>NQ-<i>p</i>-PTZ</b>	-5.41	-3.63	1.78
<b>NQ-<i>m</i>-PTZ</b>	-5.31	-3.56	1.75

<sup>a</sup> Measurements were performed for 1 mM solutions of investigated compounds in the presence of 100 mM tetrabutylammonium tetrafluoroborate and calibrated using ferrocene/ferrocenium redox couple.

**DQ-PTZ**, **NQ-*p*-PTZ** and **NQ-*m*-PTZ** exhibited reversible two-step reduction according to the two quinoxaline or phenazine units and one step oxidation process, indicating their high electrochemical stabilities suitable for carrier injection/transportation in optoelectronic materials. The HOMO and LUMO were estimated by the oxidation potential and the first reduction potential, respectively. The HOMO-LUMO energy gap ( $E_g$ ) for **DQ-PTZ** (2.03 eV) was higher than for **NQ-*p*-PTZ** (1.78 eV) and **NQ-*m*-PTZ** (1.75 eV). The compound **DQ-PXZ** showed a similar profile in the CV, displaying reversible two-step reduction and one-step reversible oxidation process. We observe that **DQ-PXZ** displayed the estimated HOMO energy (-5.39 eV) a little lower than **DQ-PTZ** (-5.35 eV), as expected due to stronger electron-donating character of phenothiazine. The compounds **DQ-DDA** and **DQ-IMD** showed more irreversible character in the reduction and oxidation process.

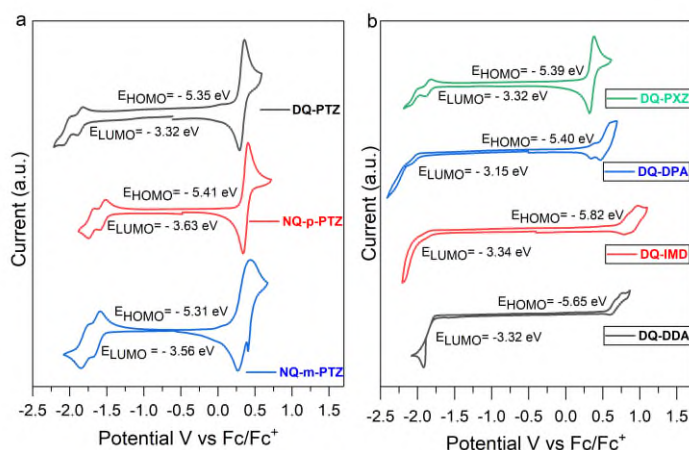


**Figure 4.** Cyclic voltammograms of a single scan of 1 mM of compounds a) **DQ-PTZ**, **NQ-*p*-PTZ** and **NQ-*m*-PTZ**; b) **DQ-PXZ**, **DQ-DPA**, **DQ-IMD** and **DQ-DDA**.

The CV curves for the compounds **DQ-DPA**, **DQ-DMAC** and **DQ-DPAC** are shown in **Figure 5**. **DQ-DPA** showed more irreversible character of the reduction process with estimated LUMO energy of -3.15 eV. While the compounds **DQ-DMAC** and **DQ-DPAC**, display more reversible character with estimated LUMO energies of -3.54 eV and -3.65 eV, respectively. For the first oxidation potentials it was possible to estimate the HOMO energies, where DPA showed first oxidation at lower potentials than DMAC and DPAC.

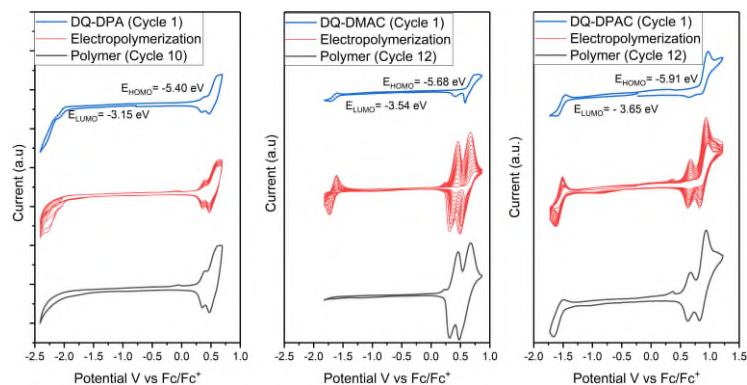


**Figure 5.** Cyclic voltammetry of 1mM of **DQ-DPA**, **DQ-DMAC** and **DQ-DPAC** in DCM  $Bu_4NBF_4$  (0.1 M) electrolyte with different potential boundaries. First cycle monomer in (blue line); electropolymerization in red and the electrochemically obtained polymer as last cycle in black.

These compounds additionally showed electrochemical polymerization process when we increment the number of cycles in CV measurements, where it can be noticed in the second and following scans the emergence of new peaks at lower potentials. The presence of new peaks is an indicative of electrochemical reactions forming new species in the electrochemical cell. If we compare the oxidation potentials of monomer and the formed species, we observe the lower oxidation potential, that indicates a higher conjugation degree of the formed polymer in relation to the monomers. Also, the increases in current during the additional scans suggest the electrodeposition of the materials on the electrode's surface.

**Table 7** shows the photoluminescence (PL) behavior for the compounds **DQ-NQ-donors** in the solvatochromism studies from less polar to more polar solvents. The emitters exhibit a wide range of accessible colors from blue to orange-red bands in PL spectra, depending on the donors attached and the polarities of the solvents. For the compounds **DQ-DPA**, **DQ-DDA** and **DQ-IMD** we observe a clear redshift from MCH to ACN, ranging from green to orange ( $\lambda_{PL}$ = 470-600 nm), indicating the strong  $^1CT$  character of  $S_1$  states that are sensible to solvents polarities being stabilized in more polar solvents. **DQ-PXZ** showed different behavior in less polar and more polar solvents. From MCH ( $\lambda_{PL(MCH)}$ = 521nm) to TOL ( $\lambda_{PL(TOL)}$ = 594 nm) we observe clear redshift in PL spectra, that is consistent with stabilization of  $^1CT$  states. In contrast to the more polar THF ( $\lambda_{PL(THF)}$ = 434 nm) where we observe a blue shift, that can be attributed to aggregation effects by restriction of intramolecular motion in more polar solvents. **DQ-DMAC** and **DQ-DPAC** showed a redshift from MCH to DCM ranging from green to orange-red (530-650 nm), suggesting the stabilization of  $^1CT$  states. These compounds were not emissive in ACN indicating the quenching of  $^1CT$  states in very polar solvents. Additionally, we observe a redshift in the solvatochromism for **DQ-PTZ** from MCH ( $\lambda_{PL(MCH)}$ = 555 nm) to ACN ( $\lambda_{PL(ACN)}$ = 618 nm). While for the compounds **NQ-p-PTZ** and **NQ-m-PTZ** the emission was quenched in more polar solvents. But we still can observe a redshift from MCH to TOL. The difference between diquinoxaline (DQ) and bisphenazine (NQ) can be observed if we compare the emission in toluene, being redshifted from **DQ-**

**PTZ** ( $\lambda_{\text{PL(TOL)}}$ = 606 nm) to **NQ-*p*-PTZ** ( $\lambda_{\text{PL(TOL)}}$ = 667 nm), indicating the more twisted donor attached to the acceptor core.

**Table 7.** Summary of photophysical characteristics of the studied **DQ-donors** and **NQ-donors**.

Compounds	$\lambda_{\text{Abs/nm}}$ [ $\epsilon/10^3\text{M}^{-1}\text{cm}^{-1}$ ] <sup>a</sup>	$\lambda_{\text{Em}}$ [nm] MCH	$\lambda_{\text{Em}}$ [nm] TOL	$\lambda_{\text{Em}}$ [nm] THF	$\lambda_{\text{Em}}$ [nm] DCM	$\lambda_{\text{Em}}$ [nm] ACN	PLQY (%)	Increase <sup>b</sup>	PLQY X Increase
<b>DQ-PTZ</b>	257, [121], 378 [11.6], 421 [6.09]	555	606	600	606	618	7.7 <sup>b</sup> ; 9.3 <sup>c</sup> ; 34 <sup>d</sup>	1.93	14.9 <sup>b</sup>
<b>DQ-PXZ</b>	263 [26.4], 270 [27.1], 289 [19.5], 328 [13.1], 375 [12.4]	521	594	434	463	463	17.7 <sup>b</sup> ; 9.6 <sup>c</sup> ; 36.5 <sup>d</sup>	2.03	35.9 <sup>b</sup>
<b>DQ-DPA</b>	263 [23.9], 269 [23.9], 305 [26.4], 334 [20.1], 440 [16.6]	473	497	536	557	575	59.9 <sup>b</sup> ; 17.6 <sup>c</sup> ; 32.4 <sup>d</sup>	1.09	65.3 <sup>b</sup>
<b>DQ-IMD</b>	262 [31.6], 269 [29.0], 287 [21.3], 420 [23.8]	525	543	554	557	579	8.1 <sup>b</sup> ; 14.3 <sup>d</sup>	1.16	9.4 <sup>b</sup>
<b>DQ-DDA</b>	262 [33.4], 268 [29.3], 313 [14.7], 429 [27.3]	508	542	561	566	584	24.5 <sup>b</sup>	1.28	31.4 <sup>b</sup>
<b>DQ-DMAC</b>	262 [22.4], 269 [23.4], 284 [23.8], 325 [37.7], 357 [11.6], 450 [2.97]	539	593	629	651	-	6.1 <sup>b</sup>	2.04	12.4 <sup>b</sup>
<b>DQ-DPAC</b>	293 [25.8], 326 [49.7], 358 [13.8], 444 [4.35]	527	559	604	630	-	14.7 <sup>b</sup>	1.52	22.3 <sup>b</sup>
<b>NQ-<i>p</i>-PTZ</b>	259 [46.4], 308 [20.8], 422 [11.0], 467 [6.37]	587	667	-	-	-	9.0 <sup>b</sup>	2.24	20.1 <sup>b</sup>
<b>NQ-<i>m</i>-PTZ</b>	258 [75.6], 306 [28.7], 423 [19.0]	610	656	-	-	-	2.4 <sup>b</sup>	3.21	7.68 <sup>b</sup>

<sup>a</sup> in DCM 0.01 mM; <sup>b</sup> in toluene 0.01 mM; <sup>c</sup> in zeonex matrix; <sup>d</sup> in CBP matrix.

To investigate the possibility of TADF behavior, measurements were realized in air-equilibrated and vacuum conditions in order to observe if oxygen is quenching excited triplet states.<sup>47</sup> **Figure 6** shows the PL spectra in the air conditions (black lines) and in vacuum conditions (red lines). We observe an increase in PL intensity in vacuum conditions for all compounds. This behavior indicates that excited triplet states are involved in the mechanism of light emission, and are quenched by oxygen.<sup>48</sup> The removal of oxygen from the system allows efficient RISC process that support TADF properties. The compounds **DQ-DPA**, **DQ-DDA** and **DQ-IMD** showed smaller PL increases in comparison with the

other compounds, varying from 1.09x, 1.16x and 1.28x, respectively. This suggests that weaker electron donors attached in the diquinoxaline cause small contribution of delayed fluorescence. Otherwise, the compounds with donors with more electron-donating ability implies in the increase of PL intensity in vacuum conditions, up to 3.2x for **NQ-*m*-PTZ**. **NQ-*p*-PTZ** and **DQ-PTZ** display an increase in the PL intensity up to 2.2x and 1.9x, suggesting that the bisphenazine core (NQ) implies more contribution of delayed fluorescence. **DQ-PXZ** and **DQ-DMAC** showed an increment in PL intensity up to 2x, which demonstrates their good usability as electron donors in TADF design.

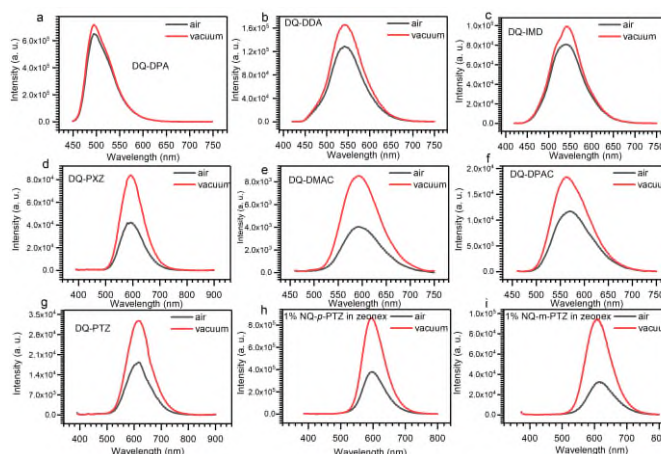


**Figure 6.** Photoluminescence (PL) spectra of **DQ-donors** in toluene solutions under air conditions (black line) and under vacuum conditions (red line). For **NQ-*p*-PTZ** and **NQ-*m*-PTZ**, in 1% of the compounds in zeonex matrix.

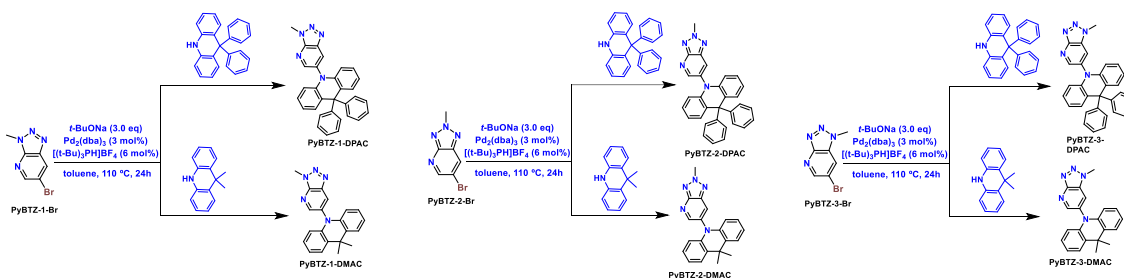
### ***D-A compounds derived from asymmetric pyridine benzotriazoles isomers: synthesis, electrochemical and photophysical characterization***

The processability in OLEDs is positively influenced by organic emitters with low molecular mass due to easy thermal evaporation or application in solution processable techniques, which avoids the high costs of device preparation.<sup>49,50</sup> In this way, the development of new low molecular mass organic emitters with a rational synthetic approach is one of the main challenges of the field, due to the market demand focusing on purely organic emitters.<sup>51,52</sup> Different acceptors were investigated to be used in TADF/RTP OLEDs such as phenazines,<sup>20,21</sup> quinoxalines,<sup>55</sup> triazines,<sup>56</sup> connected with different donor moieties. These acceptor units presents N-rich systems that can increase the electron-acceptor character and favor the spin-orbit coupling, being an alternative to the use of heavy atoms from phosphorescent emitters.<sup>58</sup> Other designs focusing on the increment of the electron-accepting character, with the use of an additional nitrogen-containing pyridinium ring, to increase the electronegativity in the system, have also been developed.<sup>60</sup>

Triazole is a five-membered ring with three nitrogen atoms which can promote the higher electron acceptor ability. Due to their versatility in synthesis, the triazole derivatives have been largely explored, mainly in medicinal chemistry because of their biological activity<sup>61–63</sup> but also in materials

science with applications in liquid crystals design.<sup>65</sup> On the other hand, their use as an acceptor core in emitters layers of TADF-based OLED devices has not been explored so far, which opens possibilities to be investigated in this field. In this way, this chapter focuses on the use of the triazole ring fused with a pyridine ring aiming to increase the electron acceptor behavior. To understand the relationship between structure and photophysical behavior, three isomers derived from [1,2,3]triazolo[4,5-*b*]pyridine (**PyBTZ**) were investigated. In these isomers, a methyl group is attached in three different positions of the triazole ring, therefore different dipole moments in the acceptor units are obtained. Thus it is possible to obtain unrealized D-A compounds derived from [1,2,3]triazolo[4,5-*b*]pyridine connected with usual donors, such as dimethyl acridine (DMAC) and diphenyl acridine (DPAC), in position 6 of the pyridine ring. The study of regioisomers of **PyBTZ** can be a great strategy to evaluate the options for different applications, since they provide a wide range of structural and electronic properties.

**Scheme 6** shows the synthetic route to obtain the **PyBTZ-1,2,3-donors** compounds. The donors were attached by palladium catalyzed N-C coupling of Buchwald-Hartwig reaction **DMAC** and **DPAC** as donor moieties. Obtaining the target compounds in excellent yields (82-96%) after purification by column chromatography.



**Scheme 6.** Synthetic route to obtain D-A compounds derived from the isomers of the [1,2,3]triazolo[4,5-*b*]pyridine core.

The electrochemical properties of **PyBTZ-1,2,3-donors** were investigated by cyclic voltammetry (CV) to estimate the HOMO and LUMO energy levels from IP and EA. The results are summarized in **Table 8**.

**Table 8.** HOMO and LUMO energy levels obtained from CV measurements of **PyBTZ-1,2,3-donors**.

Compound	Cyclic Voltammetry <sup>a</sup>		
	HOMO (eV)	LUMO (eV)	$E_g$ (eV)
<b>PyBTZ-1-DMAC</b>	-5.90	-3.10	2.80
<b>PyBTZ-2-DMAC</b>	-5.83	-3.15	2.68
<b>PyBTZ-3-DMAC</b>	-5.98	-3.23	2.75
<b>PyBTZ-1-DPAC</b>	-5.97	-3.10	2.87
<b>PyBTZ-2-DPAC</b>	-5.97	-3.14	2.83
<b>PyBTZ-3-DPAC</b>	-6.05	-3.23	2.82

<sup>a</sup> Measurements were performed for 1 mM solutions of investigated compounds in the presence of 100 mM tetrabutylammonium tetrafluoroborate and calibrated using ferrocene/ferrocenium redox couple.

All materials showed good stability in the applied voltage range, with non-reversible reduction process taking place on the pyridine benzotriazole ring. The LUMO energy levels were similar in values for all compounds. But appears to be affected by the position of the methyl group in the triazole ring. The oxidation process also appears as irreversible, taking place on the donor moieties (DMAC and DPAC). All compounds showed not reversible reduction and oxidations process. The highest value of energy of LUMO obtained for DMAC derivatives was for **PyBTZ-1-DMAC** (-3.10 eV) and for the compounds with DPAC as donor, the highest energy of LUMO was obtained for the compound **PyBTZ-1-DPAC** (-3.10 eV). Indicating that the isomer 1, implies in the reduction process in lower potentials, following the sequence 1>2>3. The estimated energies of HOMO were more affected by the change from the donor DMAC to DPAC than the variation of the isomer with same donor, which was expected due to difference in the strength of electron-donation. The variations of donor moieties and the position of the methyl group on the triazole ring implies changes in the HOMO-LUMO gap ( $E_g$ ). This indicates that the D-A combinations are very important in  $E_g$  modulation for which both, the strength of the donor and the variation of the isomer are important.

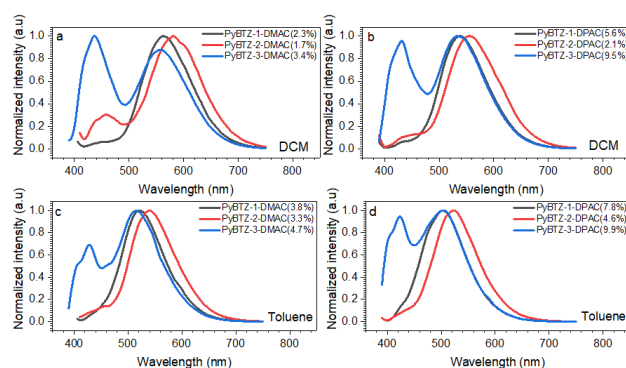


**Figure 7.** Photoluminescence (PL) spectra of the compounds **PyBTZ-1,2,3-donors** in DCM and TOL solutions 0.1 mM.

**Table 9** and **Figure 7** show the photoluminescence behavior for the variation of isomers and donors different solvents. Considering the same donor attached, we observe a similar gaussian shape of the emission characteristic of  $^1\text{CT}$  emission for the isomers 1 and 2. We also observe a red shift from 1 to 2, and additionally a clearly different profile of emission for the isomer 3, displaying two emission bands, more evident in DCM than TOL. This behavior suggests the mixture  $^1\text{LE}+^1\text{CT}$  character of the transition  $S_1 \rightarrow S_0$  for the isomer 3, with maximum wavelengths in DCM centered at 437 and 556 nm for **PyBTZ-3-DMAC**, and at 421 and 504 nm for **PyBTZ-3-DPAC**. Also is possible to observe two emission bands for these compounds in TOL solutions, but with the first less intense, indicating the stabilization of the  $^1\text{CT}$  emission with the change in the polarities of solvent. The PLQY in air conditions measured at DCM and TOL, showed an increase in less polar solvents, indicating the polarity quenching of  $^1\text{CT}$  states.

**Table 9.** Summary of photophysical characteristics of the studied **PyBTZ-1,2,3-Donors** compounds.

Compounds	$\lambda_{\text{Abs}}/\text{nm}$ [ $\epsilon/10^3\text{M}^{-1}\text{cm}^{-1}$ ] <sup>a</sup>	$\lambda_{\text{Em}}$ [nm] MCH	$\lambda_{\text{Em}}$ [nm] TOL	$\lambda_{\text{Em}}$ [nm] THF	$\lambda_{\text{Em}}$ [nm] DCM	$\lambda_{\text{Em}}$ [nm] ACN	PLQY [%] DCM/TOL
PyBTZ-1-DMAC	277 [11.0], 391 [0.4]	514	520	534	565	576	2.3/3.8
PyBTZ-2-DMAC	284 [9.15], 400 [0.3]	529	539	555	581	457; 597	1.7/3.3
PyBTZ-3-DMAC	282 [8.9], 392 [0.3]	424; 512	428; 518	431; 541	437; 556	438; 580	3.4/4.7
PyBTZ-1-DPAC	288 [9.7], 381 [0.5]	497	502	516	538	550	5.6/7.8
PyBTZ-2-DPAC	288 [8.2], 391 [0.5]	513	524	538	556	573	2.1/4.6
PyBTZ-3-DPAC	284 [10.8], 382 [0.6]	421; 504	422; 503	424; 516	431; 538	431; 544	9.5/9.9

### *D-A regioisomers derived from benzopyridoimidazoisoquinolinone and phosphanimine cores: design, synthesis and photophysical/electrochemical properties*

Materials based on N-rich acceptor cores based on imidazoquinolinones have been largely investigated for application in optoelectronic devices due to their high level of charge transport carriers.<sup>66</sup> Imidazoisoquinolinone can be prepared by the dehydration reaction between *ortho*-diamino compounds and anhydrides. They have a high acceptor character due to the presence of the nitrogen atom and the carbonyl group in the system, which increases the electronegativity in the core.<sup>67</sup>

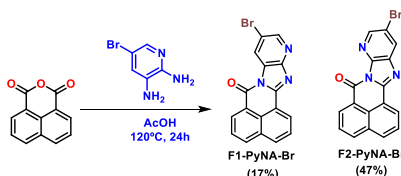
The condensation with the use of asymmetric aromatic diamines leads to isomers in different ratios. These results are due to the electron-donating/withdrawing behavior of the functional groups in the aromatic part of diamine, which affects the nucleophilicity of the amino group. Thus, electron-donating groups (EDG) in *ortho* or *para* positions in the diamine lead to strong nucleophilicity of the diamine helping to increase the reaction yield. On the other hand, electron-withdrawing groups (EWG) in *ortho* or *para* positions decrease the reactivity and promote the formation of isomers with carbonyl group and EWG on opposite sides of the molecule, as demonstrated by Anzenbacher and co-authors.<sup>68</sup>

The chemistry of organophosphorus has been largely studied in different areas. Related to materials science the application of these materials is not very explored mainly due to the poor stability of the C=P and P=P bonds.<sup>69</sup> Just some classes of organophosphorus, such as triaryl phosphines, phospholes, and phosphazenes, have good stability that allows for use in optoelectronics devices. Large part of these applications were based on the use of organophosphorus transition metal ligands, for example.<sup>70</sup> Other classes of P-based compounds, such as phosphazenes (or phosphanimines) are organic compounds where P and N atoms are linked through a double bond (P=N).<sup>71</sup> Due to the high polarity of the bond, there is no evidence of conjugation in phosphazenes because they behave as ylides. These materials present good thermal and hydrolytic stability. Which makes them investigated in applications as emitters for OLEDs and as electrolytes for dye-sensitized solar cells (DSSCs). Similarly, to P=O systems, applications as hosts were also explored. In literature, research focusing in the use of triphenyl-phosphanimine are not very explored.<sup>72</sup> The presence of the triphenyl group connected with P=N can

enhance the conjugation degree in the molecular structure. In this way the connection of the triphenyl-phosphanimine ( $\text{Ph}_3\text{P}=\text{N}$ ) with common electron-donors used in TADF systems was not explored so far. The design of new  $\text{Ph}_3\text{P}=\text{N}$  based compounds can be an excellent strategy to obtaining multifunctional materials for optoelectronic applications.

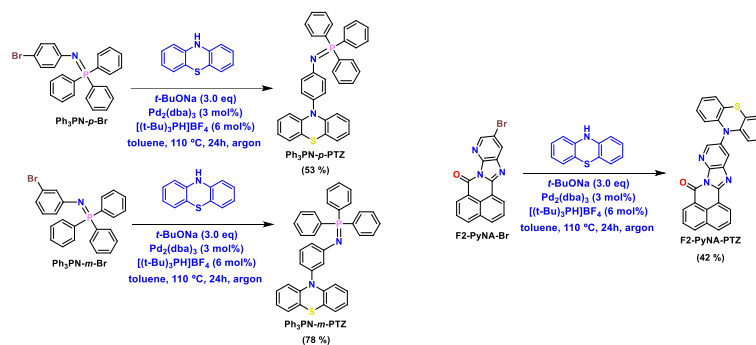
Based on that, this chapter will show the design and synthesis of two different regioisomers cores, both connected with a common donor phenothiazine. One core based on triphenyl-phosphanimine ( $\text{Ph}_3\text{PN}$ ) with phenothiazine connected in *para* and *meta* positions, to evaluate the electrochemical and photophysical properties for suitability in optoelectronics applications. The other system based on benzopyridoimidazoquinolinone ( $\text{PyNA}$ ) as acceptor core, also connected with phenothiazine, to investigate the electrochemical and photophysical behavior.

The benzimidazole isomers  $\text{PyNA-Br}$  were synthesized based on the condensation reaction of naphthalic anhydride and 2,3-diamino-5-bromopyridine (**Scheme 7**). As an asymmetric diamine was used, the reaction gave two isomers in a ratio of 7:3, with 72% yield for the mixture of isomers. The isomers were separated by chromatography column using a gradient chloroform/hexane (6:1) to pure chloroform as eluent. As for 2,3-diamino-5-bromopyridine, the pyridine nitrogen is *ortho* to diamine, the majority product from the condensation reaction presents the carbonyl group and pyridine nitrogen to the same side and consequently the bromine to opposite side to carbonyl group (**F2-PyNA-Br**), which was consistent with the yields of the regio-isomers.



**Scheme 7.** Synthesis of bromo-benzopyridoimidazoquinolinone isomers **F1,F2-PyNA-Br**.

The synthesis of the phosphanimine cores follows typical procedures from literature.<sup>73</sup> The first step was related to formation of aryl azides by reaction of formation of diazonium salts in *para* and *meta* bromo-aryl amines followed by a substitution using sodium azide. The second step was based on the reaction of bromo-aryl azide with triphenylphosphine to obtain the *para* and *meta* brominated triphenyl-phosphanimine cores ( $\text{Ph}_3\text{PN-}p,m\text{-Br}$ ) in excellent yields. The brominated cores were used as substrate in the N-C Buchwald-Hartwig cross-coupling reactions using phenothiazine as donors moieties. The conditions are shown in the **Scheme 8**. For  $\text{Ph}_3\text{PN-}p\text{-PTZ}$  and  $\text{Ph}_3\text{PN-}m\text{-PTZ}$  were obtained in 53% and 78% of yield, respectively. Related with PyNA core, was performed the N-C coupling with the two isomers in same conditions, but **F1-PyNA-Br** did not react with phenothiazine in these conditions. The non-reaction in **F1-PyNA-Br** suggests that the carbonyl and bromine for same side in the molecule difficult the connection of phenothiazine due to steric hindrance. For the other side, **F2-PyNA-PTZ** was obtained in moderate yield (42%) after purification by chromatograph column. Indicating that the bromine and carbonyl group in opposite sides increases the reactivity.



**Scheme 8.** Synthetic route used to obtain the regioisomers compounds derived from phosphanimine and benzopyridoimidazoquinolinone cores.

The optical properties of the **Ph<sub>3</sub>PN-*p,m*-PTZ** compounds in the aggregate were investigated in THF/water mixtures with different water fractions ( $f_w$ ) at 0.1 mM concentration. The experimental results and photographs (**Figure 8**) show that the emission spectra of the compounds show similar behavior in THF/water mixtures. **Ph<sub>3</sub>PN-*p*-PTZ** and **Ph<sub>3</sub>PN-*m*-PTZ** display very low emission in THF solutions, while the emission is increased upon addition of water ( $f_w = 80$ -90%) indicating evident aggregation induced emission enhancement (AIEE) behavior.

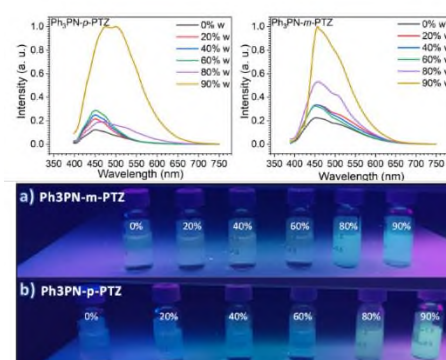


**Figure 8.** Aggregation studies of the compounds **Ph<sub>3</sub>PN-*p*-PTZ** and **Ph<sub>3</sub>PN-*m*-PTZ** in different water fractions ( $f_w$ ) in THF solution 0.1 mM.

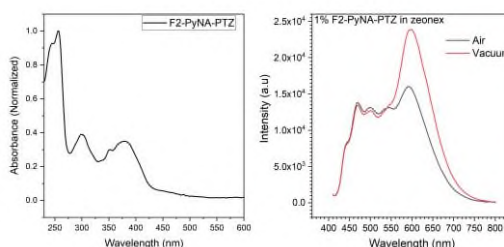


**Figure 9.** Absorption spectra in DCM solution 0.01 mM and PL spectra in air equilibrated and under vacuum of 1% of the compound **F2-PyNA-PTZ** in Zeonex matrix.

The **Figure 9** shows the UV-Vis absorption in DCM and PL spectra in zeonex matrix at air equilibrated and vacuum conditions of the compound **F2-PyNA-PTZ**. We can observe strong absorption band around 250 nm, that can be signed to the  $\pi \rightarrow \pi^*$  transitions from aromatic systems related to

benzopyridoimidazoquinolinone core (PyNA).<sup>66</sup> We can note less intense broad absorption band around 380 nm, that can be attributed to the CT transitions from the donor unit to the acceptor core.<sup>74</sup> The photoluminescence behavior was investigated under air and vacuum condition and we can note the increase of PL intensity under vacuum indicating that triplet of excited states are involved in the mechanism of emission. Also we can note that the PL emission displays very large broad band with maximums wavelengths varying from 468 to 600 nm. This behavior leads to emission close to white, which is an interesting photophysical behavior.

## General conclusions

This thesis describes the design and synthesis of several series of multifunctional compounds belonging to distinct classes of compounds. In total, 35 unprecedented molecules were designed and synthesized, with full structure characterization by NMR and HRMS. The Pd-catalyzed reactions, such as N-C and C-C cross-coupling, were the base reactions to connect electron-donors and electron-acceptors in different arrangements, such as D-A, D-A-D and D-A-A-D. The synthesis of the electron acceptors covered a wide range of chemical reactions. The chemistry of quinoxalines, perylene, benzotriazoles, phosphanimine, and benzimidazoles was used to obtain functional materials.

Additionally, electrochemical and photophysical behavior were investigated in order to check the suitability of the new materials for optoelectronics applications. The electrochemical and photophysical properties were controlled by different molecular designs, where common electron-donors were connected to new acceptors to be investigated. The materials present different behaviors, depending on the core, regioisomers, and donors attached. It was observed that N-rich electron acceptors such as quinoxaline are attractive candidates to be connected with strong to moderate electron donors, such as phenothiazine, phenoxazine, and acridine derivatives to have the possibility of TADF properties, due to a strong CT character. On the other side, weaker donors such as diphenylamine, azepine derivatives, and carbazoles imply a more substantial HOMO-LUMO overlap, which decreases the TADF behavior.

## References

- 1 Y. Huang, et al, *Light Sci. Appl.*, , DOI:10.1038/s41377-020-0341-9.
- 2 J. Yao, et al, *J. Mater. Chem. C*, 2019, **7**, 11293–11302.
- 3 M. U. Chaudhry, et al, *Adv. Funct. Mater.*, 2020, **30**, 1–15.
- 4 B. Valeur and M. N. Berberan-Santos, 2012, 49–51.
- 5 G. Hong, et al, *Adv. Mater.*, , DOI:10.1002/adma.202005630.
- 6 W. P. Lustig, F. Wang, S. J. Teat, Z. Hu, Q. Gong and J. Li, *Inorg. Chem.*, 2016, **55**, 7250–7256.
- 7 P. Data and Y. Takeda, *Chem. - An Asian J.*, 2019, **14**, 1613–1636.
- 8 F. B. Dias, et al, *Methods Appl. Fluoresc.*, , DOI:10.1088/2050-6120/aa537e.
- 9 T. Zhang, Yet al, *Angew. Chemie Int. Ed.*, 2023, **17**, 955.

- 10 X. Liang, Z. L. Tu and Y. X. Zheng, *Chem. - A Eur. J.*, 2019, **25**, 5623–5642.
- 11 Z. Yang, Zet al, *Chem. Soc. Rev.*, 2017, **46**, 915–1016.
- 12 M. Godumala, et al, *J. Mater. Chem. C*, 2019, **7**, 2172–2198.
- 13 L. Zhan, et al, *Angew. Chemie - Int. Ed.*, 2019, **58**, 17651–17655.
- 14 Z. Xu, D. Hean, C. Climent, D. Casanova and M. O. Wolf, *Mater. Adv.*, 2021, **2**, 5777–5784.
- 15 D. Hall, et al, *Mater. horizons*, 2022, **9**, 1068–1080.
- 16 H. Z. Li, F. M. Xie, Y. Q. Li and J. X. Tang, *J. Mater. Chem. C*, 2023, 6471–6511.
- 17 H. Li, et al, *Chempluschem*, 2021, **86**, 95–102.
- 18 T. Huang, D. Liu, J. Jiang and W. Jiang, *Chem. - A Eur. J.*, 2019, **25**, 10926–10937.
- 19 L. Yu, Z. Wu, G. Xie, W. Zeng, D. Ma and C. Yang, *Chem. Sci.*, 2018, **9**, 1385–1391.
- 20 B. Sk, S. Sharma, A. James, S. Kundu and A. Patra, *J. Mater. Chem. C*, 2020, **8**, 12943–12950.
- 21 F. M. Xie, et al, *ACS Appl. Mater. Interfaces*, 2019, **11**, 26144–26151.
- 22 L. Yu and C. Yang, *J. Mater. Chem. C*, 2021, **9**, 17265–17286.
- 23 G. H. Kim, et al, *Mater. Horizons*, 2017, **4**, 619–624.
- 24 T. Goya, et al, *Asian J. Org. Chem.*, 2022, **11**, 1–7.
- 25 C. M. Cardona, et al, *Adv. Mater.*, 2011, **23**, 2367–2371.
- 26 M. Urban, et al, *Angew. Chemie Int. Ed.*, , DOI:10.1002/anie.202217530.
- 27 P. Data, et al, *Angew. Chemie - Int. Ed.*, 2016, **55**, 5739–5744.
- 28 Y. Hong, J. W. Y. Lam and B. Z. Tang, *Chem. Commun.*, 2009, 4332.
- 29 Y. Liu, S. et al, *J. Mater. Chem.*, 2012, **22**, 5184–5189.
- 30 Z. Yang, et al, *J. Mater. Chem.*, 2010, **20**, 7352–7359.
- 31 M. Cekaviciute, et al, *Molecules*, , DOI:10.3390/molecules25030445.
- 32 C. Li and H. Wonneberger, *Adv. Mater.*, 2012, **24**, 613–636.
- 33 M. Zhu, Y. Chen, H. Guo, F. Yang and X. Song, *New J. Chem.*, 2018, **42**, 8998–9005.
- 34 C. Huang, S. Barlow and S. R. Marder, *J. Org. Chem.*, 2011, **76**, 2386–2407.
- 35 R. K. Dubey, et al, *Chem. Sci.*, 2016, **7**, 3517–3532.
- 36 R. R. Reghu, et al, *J. Mater. Chem.*, 2011, **21**, 7811–7819.
- 37 M. Imran, et al, *J. Mater. Chem. C*, 2020, **8**, 8305–8319.
- 38 A. G. Macedo, et al, *J. Mater. Sci. Mater. Electron.*, 2019, **30**, 15803–15824.
- 39 A. Nowak-Król and F. Würthner, *Org. Chem. Front.*, 2019, **6**, 1272–1318.
- 40 N. Pearce, E. S. Davies and N. R. Champness, *Dye. Pigment.*, 2020, **183**, 108735.
- 41 M. Gao, et al, *Nanomaterials*, , DOI:10.3390/nano12234117.
- 42 M. Okazaki, et al, *Chem. Sci.*, 2017, **8**, 2677–2686.
- 43 P. Data and Y. Takeda, *Chem. - An Asian J.*, 2019, **14**, 1613–1636.
- 44 J. X. Chen, Yet al, *J. Mater. Chem. C*, 2020, **8**, 13263–13269.
- 45 W. Wang, et al, *Dye. Pigment.*, 2023, **218**, 111444.
- 46 E. Chatir, et al, *Chem. - A Eur. J.*, , DOI:10.1002/chem.202103755.

- 47 S. Kumar, et al, *J. Phys. Chem. Lett.*, 2021, **12**, 2820–2830.
- 48 K. L. Woon, et al, *J. Phys. Chem. C*, 2019, **123**, 12400–12410.
- 49 T. Huang, W. Jiang and L. Duan, *J. Mater. Chem. C*, 2018, **6**, 5577–5596.
- 50 Y. Zou, S. Gong, G. Xie and C. Yang, *Adv. Opt. Mater.*, 2018, **6**, 1800568.
- 51 M. Y. Wong and E. Zysman-Colman, *Adv. Mater.*, , DOI:10.1002/adma.201605444.
- 52 Z. Chen, et al, *Adv. Sci.*, 2023, 2207003.
- 53 L. Yu, et al, *J. Mater. Chem. C*, 2020, **8**, 12445–12449.
- 54 T. Hosono, et al, *J. Mater. Chem. C*, 2022, **10**, 4905–4913.
- 55 X. Y. Wang, et al, *New J. Chem.*, 2022, 18854–18864.
- 56 R. Braveenth, et al, *J. Mater. Chem. C*, 2019, **7**, 7672–7680.
- 57 T. Matulaitis, et al, *J. Phys. Chem. C*, 2017, **121**, 23618–23625.
- 58 K. Rayappa Naveen, et al, *Chem. – A Eur. J.*, , DOI:10.1002/chem.202103532.
- 59 M. Hempe, et al, *J. Phys. Chem. Lett.*, 2022, **13**, 8221–8227.
- 60 T. Huang, D. Liu, J. Jiang and W. Jiang, *Chem. – A Eur. J.*, 2019, **25**, 10926–10937.
- 61 G. Zoidis, et al, *ChemMedChem*, 2021, **16**, 134–144.
- 62 D. P. Vala, et al, *ACS Omega*, 2022, **7**, 36945–36987.
- 63 A. Lauria, et al, *European J. Org. Chem.*, 2014, **2014**, 3289–3306.
- 64 G. Y. Yeap, et al, *New J. Chem.*, 2013, **37**, 1906–1911.
- 65 N. Gimeno, et al, *J. Mater. Chem.*, 2012, **22**, 16791–16800.
- 66 S. R. Nayak, et al, *J. Phys. Chem. C*, 2023, 127, 10291–10302.
- 67 U. Yildiz, et al, *Mol. Biol. Rep.*, 2020, **47**, 1563–1572.
- 68 M. Mamada, et al, *Chem. - A Eur. J.*, 2014, **20**, 11835–11846.
- 69 D. A. Smith, et al, *Angew. Chemie Int. Ed.*, 2009, **48**, 9109–9113.
- 70 S. Ullrich, et al, *Angew. Chemie Int. Ed.*, 2019, **58**, 10335–10339.
- 71 P. Rotering, L. F. B. Wilm, J. A. Werra and F. Dielmann, *Chem. - A Eur. J.*, 2020, **26**, 406–411.
- 72 D. Joly, P. A. Bouit and M. Hissler, *J. Mater. Chem. C*, 2016, **4**, 3686–3698.
- 73 A. C. Savva, et al, *J. Org. Chem.*, 2017, **82**, 7564–7575.
- 74 H. Zhang, et al, *Macromolecules*, 2019, **52**, 9364–9375.